

Ligand effects on Ni^{II}-catalysed alkane-hydroxylation with *m*-CPBA†

Takayuki Nagataki, Kenta Ishii, Yoshimitsu Tachi and Shinobu Itoh*

Received 25th October 2006, Accepted 18th January 2007

First published as an Advance Article on the web 6th February 2007

DOI: 10.1039/b615503k

Nickel(II) complexes supported by a series of pyridylalkylamine ligands [tris(2-pyridylmethyl)amine (TPA; complexes **1a** and **1b**), tris[2-(2-pyridyl)ethyl]amine (TEPA; complexes **2a** and **2b**), 6-[*N,N*-bis(2-pyridylmethyl)aminomethyl]-2,4-di-*tert*-butylphenol (^{Dtbp}Pym2H; complexes **3a** and **3b**), 6-[*N,N*-bis[2-(2-pyridyl)ethyl]aminomethyl]-2,4-di-*tert*-butylphenol (^{Dtbp}Pye2H; complexes **4a** and **4b**), *N*-benzyl-bis(2-pyridylmethyl)amine (^{Bz}Pym2; complex **5a**) and *N*-benzyl-bis[2-(2-pyridyl)ethyl]amine (^{Bz}Pye2; complex **6a**)] have been synthesized and structurally characterized by X-ray crystallographic analysis [coordinating counter anion (co-ligand) of complexes **na** (*n* = 1–6) is AcO[−] and that of complexes **nb** (*n* = 1–4) is NO₃[−]]. All complexes, except **1b**, were obtained as a mononuclear nickel(II) complex exhibiting a distorted octahedral geometry, whereas complex **1b** was isolated as a dinuclear nickel(II) complex bridged by two nitrate anions. Catalytic activity of the nickel(II) complexes were examined in the oxidation of cyclohexane with *m*-CPBA as an oxidant. In all cases, the oxygenation reaction proceeded catalytically to give cyclohexanol as the major product together with cyclohexanone as the minor product. The complexes containing the pyridylmethylamine (Pym) metal-binding group (**1a**, **3a**, **5a**) showed higher turnover number (TON) than those containing the pyridylethylamine (Pye) metal-binding group (**2a**, **4a**, **6a**), whereas the alcohol/ketone (A/K) selectivity was much higher with the latter (Pye system) than the former (Pym system). On the other hand, the existence of the NO₃[−] co-ligand (**1b**, **2b** and **3b**) caused a lag phase in the early stage of the catalytic reaction. Electronic and steric effects of the supporting ligands as well as the chemical behavior of the co-ligands on the catalytic activity of the nickel(II) complexes have been discussed on the basis of their X-ray structures.

Introduction

Development of an efficient catalyst for selective oxygenation of saturated hydrocarbons is an important research objective in synthetic and industrial organic chemistry.^{1–9} So far, a great deal of attention has been focused on heme and non-heme iron complexes as well as Mn, Co, Ru and Cu complexes.^{10–41} Recently, we have found that a simple Ni^{II}(TPA) complex [TPA: tris(2-pyridylmethyl)amine] also works as a very efficient turnover catalyst for alkane hydroxylation with *m*-CPBA (*m*-chloroperbenzoic acid) (Fig. 1).⁴²

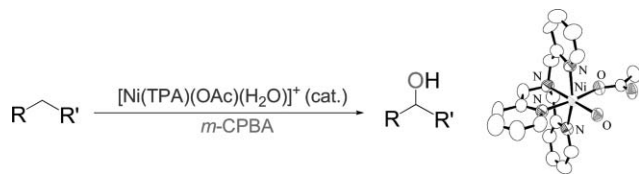


Fig. 1 Ni^{II}(TPA)-catalysed oxygenation of alkanes with *m*-CPBA.⁴²

Department of Chemistry, Graduate School of Science, Osaka City University, 3-3-138 Sugimoto, Sumiyoshi-ku, Osaka, 558-8585, Japan. E-mail: shinobu@sci.osaka-cu.ac.jp

† Electronic supplementary information (ESI) available: Summary of X-ray crystallographic data (Table S1), bond lengths and angles (Table S2), and the time courses for cyclohexane oxidation with the Ni(II) complexes (Fig. S1–S6). Atomic coordinates, thermal parameters, and intermolecular bond distances and angles are provided in CIF format. See DOI: 10.1039/b615503k

The reaction exhibited a high alcohol-product selectivity and a high regioselectivity for tertiary carbons (3°) against the secondary carbons (2°).⁴² An appreciable amount of kinetic deuterium isotope effect ($k_H/k_D = 2.8$) was also obtained.⁴² Moreover, the total TON (turnover number) of the Ni^{II} complex was higher than that of Fe^{II}, Mn^{II} and Co^{II} complexes of the same ligand, and the alcohol-product selectivity of the Ni^{II} complex was much better than that of the Fe^{II} and Mn^{II} complexes.⁴² Notably, orders of the catalytic activity (TON) (Ni^{II} > Fe^{II} > Co^{II} > Mn^{II}) and the alcohol-product selectivity (Co^{II} > Ni^{II} > Fe^{II} ≫ Mn^{II}) of the complexes in the TPA-system were similar to the orders of the efficiency and alcohol-product selectivity in the gas phase reaction of methane with the first-row metal-oxo species MO⁺ (M = Ni, Co, Fe, Mn) reported by Schwarz and co-workers.⁴³ On the basis of these results, we concluded that our reaction also involves a highly reactive metal-based oxidant such as (L)NiO⁺ rather than autooxidation type free radical species.^{5,42} In this study, we have investigated the ligand effects on the structure and catalytic activity of the Ni^{II}-complexes using a series of pyridylalkylamine derivatives shown in Chart 1. Effects of the coordinating co-ligands (counter anion) have also been examined.

Experimental

General

The reagents and the solvents used in this study except the ligand and the complexes were commercial products of the highest available purity and were further purified by standard methods,

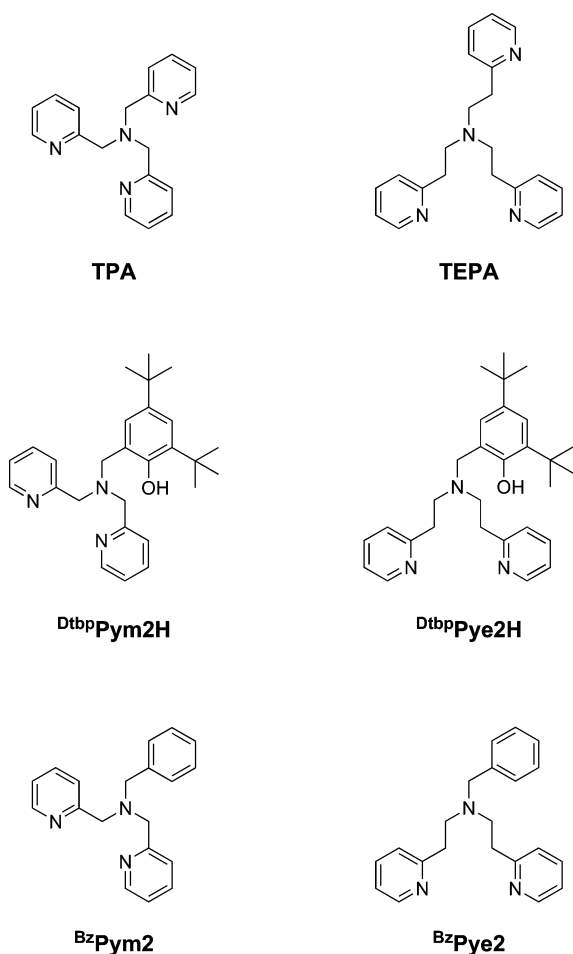


Chart 1

if necessary.⁴⁴ Tris(2-pyridylmethyl)amine (TPA), tris[2-(2-pyridyl)ethyl]amine (TEPA), *N*-benzyl-bis(2-pyridylmethyl)amine (*Bz*Pym2), *N*-benzyl-bis[2-(2-pyridyl)ethyl]amine (*Bz*Pye2), 6-[*N,N*-bis(2-pyridylmethyl)aminomethyl]-2,4-di-*tert*-butylphenol (*Dtbp*Pym2H) and 6-[*N,N*-bis[2-(2-pyridyl)ethyl]aminomethyl]-2,4-di-*tert*-butylphenol (*Dtbp*Pye2H) were synthesized according to reported procedures.^{45–50} $[\text{Ni}^{\text{II}}(\text{TPA})(\text{OAc})(\text{H}_2\text{O})]\text{BPh}_4$ (**1a**) was prepared according to the reported procedure.⁴² FT-IR spectra were recorded with a Jasco FT/IR-4100. Mass spectra were recorded with a JEOL JMS-700T Tandem MS station or a PE SCIEX API 150EX (for ESI-MS). ¹H NMR spectra were recorded on a JEOL LMN-ECP300WB or an LMX-GX400. UV-vis spectra were measured using a Hewlett-Packard HP8453 diode array spectrophotometer or a Jasco V-570. Elemental analyses were performed on a Perkin-Elmer or a Fisons instruments EA 1108 Elemental analyzer.

Synthesis

$[\text{Ni}^{\text{II}}_2(\text{TPA})_2(\mu\text{-NO}_3)_2](\text{BPh}_4)_2$ (**1b**). An ethanol solution (10 mL) of $\text{Ni}^{\text{II}}(\text{NO}_3)_2 \cdot 6\text{H}_2\text{O}$ (180.2 mg, 0.62 mmol) was added to an ethanol solution (5 mL) of TPA (179.8 mg, 0.62 mmol) with stirring at room temperature. The color of the solution turned to brown. After the solution was stirred for 1 h, NaBPh_4 (212 mg, 0.62 mmol) was added to the mixture to give a brown precipitate, which was collected by filtration, washed with ethanol

and dried. Recrystallization of the crude product from CH_2Cl_2 -cyclohexane gave pure complex **1b** as purple crystals (295 mg, 65%). FT-IR (KBr): 1439, 1317, 1285 (NO_3^-), 734, 704 cm^{-1} (BPh_4^-); HRMS (FAB⁺): m/z 410.0759 [0.5M-BPh_4]⁺, calcd for $\text{C}_{18}\text{H}_{18}\text{N}_5\text{O}_3\text{Ni}$ 410.0763; Anal. Calcd for $[\text{Ni}_2(\text{TPA})_2(\text{NO}_3)_2](\text{BPh}_4)_2$, $\text{C}_{84}\text{H}_{76}\text{N}_{10}\text{O}_6\text{Ni}_2\text{B}_2$: C, 69.08; H, 5.24; N, 9.59. Found: C, 69.06; H, 5.20; N, 9.55.

$[\text{Ni}^{\text{II}}(\text{TEPA})(\text{OAc})]\text{BPh}_4$ (**2a**). A methanol solution (5 mL) of $\text{Ni}^{\text{II}}(\text{OAc})_2 \cdot 4\text{H}_2\text{O}$ (62.3 mg, 0.25 mmol) was added to a methanol solution (5 mL) of TEPA (83.1 mg, 0.25 mmol) with stirring at room temperature. Color of the solution turned to blue. After stirring for 2 h, NaBPh_4 (86 mg, 0.25 mmol) was added to the mixture to give a pale blue precipitate, which was collected by filtration, washed with methanol and dried (159.8 mg, 83%). FT-IR (KBr): 1536, 1456 (OAc^-), 733, 707 cm^{-1} (BPh_4^-); HRMS (FAB⁺): m/z 449.1481 [M-BPh_4]⁺, calcd for $\text{C}_{23}\text{H}_{27}\text{N}_4\text{O}_2\text{Ni}$ 449.1487; Anal. Calcd for $[\text{Ni}(\text{TEPA})(\text{OAc})]\text{BPh}_4$, $\text{C}_{47}\text{H}_{47}\text{N}_4\text{O}_2\text{NiB}$: C, 73.37; H, 6.16; N, 7.28. Found: C, 73.11; H, 6.28; N, 7.09.

Single crystals suitable for X-ray crystallographic analysis were obtained by slow diffusion of cyclohexane into a CH_2Cl_2 solution of the complex.

$[\text{Ni}^{\text{II}}(\text{TEPA})(\text{NO}_3)]\text{BPh}_4$ (**2b**). A methanol solution (4 mL) of $\text{Ni}^{\text{II}}(\text{NO}_3)_2 \cdot 6\text{H}_2\text{O}$ (59.6 mg, 0.205 mmol) was added to a methanol solution (4 mL) of TEPA (68.0 mg, 0.205 mmol) with stirring at room temperature. The color of the solution turned to blue. After stirring for 2 h, NaBPh_4 (77 mg, 0.225 mmol) was added to the mixture to give a pale blue precipitate, which was collected by filtration, washed with methanol and dried (149.1 mg, 94%). FT-IR (KBr): 1493, 1277 (NO_3^-), 734, 705 cm^{-1} (BPh_4^-); HRMS (FAB⁺): m/z 452.1241 [M-BPh_4]⁺, calcd for $\text{C}_{21}\text{H}_{24}\text{N}_5\text{O}_3\text{Ni}$ 452.1232; Anal. Calcd for $[\text{Ni}(\text{TEPA})(\text{NO}_3)]\text{BPh}_4$, $\text{C}_{45}\text{H}_{44}\text{N}_5\text{O}_3\text{NiB}$: C, 69.98; H, 5.74; N, 9.07. Found: C, 70.01; H, 5.73; N, 9.10.

Single crystals suitable for X-ray crystallographic analysis were obtained by slow evaporation of an acetonitrile solution of the complex.

$[\text{Ni}^{\text{II}}(\text{DtbpPym2H})(\text{OAc})(\text{MeOH})]\text{BPh}_4$ (**3a**). A methanol solution (3 mL) of $\text{Ni}^{\text{II}}(\text{OAc})_2 \cdot 4\text{H}_2\text{O}$ (49.8 mg, 0.20 mmol) was added to a methanol solution (3 mL) of *Dtbp*Pym2H (83.5 mg, 0.20 mmol) with stirring at room temperature. The color of the solution turned to blue-green. After stirring for 2 h, NaBPh_4 (69 mg, 0.20 mmol) was added. The mixture was allowed to stand for several hours to afford blue crystals, which were collected by filtration, washed with cold methanol and dried (147.5 mg, 83%). FT-IR (KBr): 3356 (O–H, broad), 1608, 1480, 1428 (OAc^-), 733, 705 cm^{-1} (BPh_4^-); HRMS (FAB⁺): m/z 534.2255 [$\text{M-BPh}_4\text{-MeOH}$]⁺, calcd for $\text{C}_{29}\text{H}_{38}\text{N}_3\text{O}_3\text{Ni}$ 534.2266; Anal. Calcd for $[\text{Ni}(\text{DtbpPym2H})(\text{OAc})(\text{MeOH})]\text{BPh}_4 \cdot 1.5\text{MeOH}$, $\text{C}_{55.5}\text{H}_{68}\text{N}_3\text{O}_{5.5}\text{NiB}$: C, 71.32; H, 7.33; N, 4.50. Found: C, 71.26; H, 6.98; N, 4.68.

$[\text{Ni}^{\text{II}}(\text{DtbpPym2H})(\text{NO}_3)(\text{MeCN})]\text{NO}_3$ (**3b**). An ethanol solution (3 mL) of $\text{Ni}^{\text{II}}(\text{NO}_3)_2 \cdot 6\text{H}_2\text{O}$ (58.2 mg, 0.20 mmol) was added to an ethanol solution (3 mL) of *Dtbp*Pym2H (83.5 mg, 0.20 mmol) with stirring at room temperature. The color of the solution turned to blue. After stirring for 30 min, the mixture was poured into hexane (150 mL) to give a blue precipitate, which was collected by filtration and dried. Recrystallization of

the crude product from acetonitrile–ether gave pure complex **3b** as blue crystals (66.4 mg, 52%). FT-IR (KBr): 3370 (O–H, broad), 1385, 1303 (NO₃⁻); HRMS (FAB⁺): *m/z* 537.2011 [M–NO₃–MeCN]⁺, calcd for C₂₇H₃₅N₄O₄Ni 537.2012; Anal. Calcd for [Ni(^{Dtbp}Pym2H)(NO₃)(MeCN)]NO₃, C₂₉H₃₈N₆O₇Ni: C, 54.31; H, 5.97; N, 13.10. Found: C, 54.30; H, 6.01; N, 12.86.

[Ni^{II}(^{Dtbp}Pye2)(OAc)] (4a). A methanol solution (5 mL) of Ni^{II}(OAc)₂·4H₂O (124.5 mg, 0.50 mmol) was added to a methanol solution (5 mL) of ^{Dtbp}Pye2H (222.8 mg, 0.50 mmol) with stirring at room temperature. The color of the solution turned to green. After stirring for 2 h, the mixture was concentrated by evaporation. The residue was re-dissolved to CH₂Cl₂ (5 mL), and the solution was poured into hexane (80 mL) to give a pale blue precipitate, which was collected by filtration and dried (233.9 mg, 83%). FT-IR (KBr): 1606, 1552, 1483, 1445 (OAc⁻); HRMS (FAB⁺): *m/z* 561.2500 [M]⁺, calcd for C₃₁H₄₁N₃O₃Ni 561.2501; Anal. Calcd for [Ni(^{Dtbp}Pye2)(OAc)], C₃₁H₄₁N₃O₃Ni: C, 66.21; H, 7.35; N, 7.47. Found: C, 66.17; H, 7.35; N, 7.44.

Single crystals suitable for X-ray crystallographic analysis were obtained by slow diffusion of hexane into an acetone solution of the complex.

[Ni^{II}(^{Dtbp}Pye2)(NO₃)] (4b). A methanol solution (5 mL) of Ni^{II}(NO₃)₂·6H₂O (145.3 mg, 0.50 mmol) was added to a methanol solution (5 mL) of ^{Dtbp}Pye2H (222.8 mg, 0.50 mmol) with stirring at room temperature. The color of the solution turned to dark green. After stirring for 2 h, triethylamine (100 μL, 0.71 mmol) was added, and the mixture was allowed to stand for several hours to afford blue crystals, which were collected by filtration, washed with cold methanol and dried (132.5 mg, 47%). FT-IR (KBr): 1489, 1328, 1272 (NO₃⁻); HRMS (FAB⁺): *m/z* 564.2233 [M]⁺, calcd for C₂₉H₃₈N₄O₄Ni 564.2247; Anal. Calcd for [Ni(^{Dtbp}Pye2)(NO₃)], C₂₉H₃₈N₄O₄Ni: C, 61.61; H, 6.78; N, 9.91. Found: C, 61.58; H, 6.70; N, 9.93.

[Ni^{II}(^{Bz}Pym2)(OAc)₂(H₂O)] (5a). A methanol solution (3 mL) of Ni^{II}(OAc)₂·4H₂O (74.7 mg, 0.30 mmol) was added to a methanol solution (3 mL) of ^{Bz}Pym2 (86.8 mg, 0.30 mmol) with stirring at room temperature. The color of the solution turned to light-blue. After stirring for 2 h, the mixture was concentrated by evaporation. The residue was re-dissolved in CH₂Cl₂ (2 mL), and the solution was poured into hexane (30 mL) to give a pale blue precipitate, which was collected by filtration and dried (118.3 mg, 81%). FT-IR (KBr): 3000 (O–H, very broad), 1605, 1582, 1568, 1407 (OAc⁻); HRMS (FAB⁺): *m/z* 406.1055 [M–OAc–H₂O]⁺, calcd for C₂₁H₂₂N₃O₂Ni 406.1065; Anal. Calcd for [Ni(^{Bz}Pym2)(OAc)₂(H₂O)], C₂₃H₂₇N₃O₅Ni: C, 57.06; H, 5.62; N, 8.68. Found: C, 56.83; H, 5.59; N, 8.60.

Single crystals suitable for X-ray crystallographic analysis were obtained by slow diffusion of ether into a CH₂Cl₂ solution of the complex.

[Ni^{II}(^{Bz}Pye2)(OAc)(H₂O)]BPh₄ (6a). A methanol solution (3 mL) of Ni^{II}(OAc)₂·4H₂O (49.8 mg, 0.20 mmol) was added to a methanol solution (3 mL) of ^{Bz}Pye2 (63.4 mg, 0.20 mmol) with stirring at room temperature. The color of the solution turned to light-blue. After stirring for 2 h, NaBPh₄ (70 mg, 0.20 mmol) was added to the mixture to give a pale blue–green precipitate, which was collected by filtration, washed with methanol and dried. Recrystallization of the powder sample from acetone–

hexane gave a pure complex of **6a** as blue crystals (105.3 mg, 68%). FT-IR (KBr): 3371, 3268 (O–H, broad), 1543, 1444 (OAc⁻), 734, 705 cm⁻¹ (BPh₄⁻); HRMS (FAB⁺): *m/z* 434.1376 [M–BPh₄–H₂O]⁺, calcd for C₂₃H₂₆N₃O₂Ni 434.1379; Anal. Calcd for [Ni(^{Bz}Pye2)(OAc)(H₂O)]BPh₄·C₃H₆O, C₅₀H₅₄N₃O₄NiB: C, 72.31; H, 6.55; N, 5.06. Found: C, 72.18; H, 6.50; N, 5.13.

X-Ray structure determination

The single crystal was mounted on a glass-fiber. X-Ray diffraction data were collected by a Rigaku RAXIS-RAPID imaging plate two-dimensional area detector using graphite-monochromated Mo K α radiation ($\lambda = 0.71069$ Å) to $2\theta_{\max}$ of 55°. All the crystallographic calculations were performed by using Crystal Structure software package of the Molecular Structure Corporation [Crystal Structure: Crystal Structure Analysis Package version 3.7.0, Molecular Structure Corp. and Rigaku Corp. (2005)]. The structures were solved with SIR92 and refined with CRYSTALS. All non-hydrogen atoms and hydrogen atoms were refined anisotropically and isotropically, respectively. Atomic coordinates, thermal parameters, and intramolecular bond distances and angles are given in the ESI.†

CCDC reference numbers 625316–625324.

For crystallographic data in CIF or other electronic format see DOI: 10.1039/b615503k

Catalytic oxygenation of cyclohexane

All procedures of the catalytic reaction were carried out under anaerobic conditions (in a glove box, [O₂] < 1 ppm, [H₂O] < 1 ppm). Typically, complex **2a** (2 μmol) in CH₃CN–CH₂Cl₂ (1 : 1 v/v, 2 mL) was added to a CH₂Cl₂ (2 mL) solution containing cyclohexane (15 mmol), *m*-CPBA (2 mmol), and nitrobenzene (50 μmol) as an internal standard with vigorous stirring at room temperature. An aliquot of the reaction mixture was taken at a certain reaction time and quenched with PPh₃ for the GLC analysis using a Shimadzu GC-14A gas chromatograph equipped with a Restek Rtx-1701 capillary column (30 m × 0.25 mm). All peaks of interest were identified by comparison of the retention times and co-injection with the authentic samples. The products were quantified by comparison against a known amount of internal standard using a calibration curve consisting of a plot of mole ratio (moles of organic compound/moles of internal standard) versus area ratio (area of organic compound/area of standard).

Results and discussion

Structural characterization of Ni^{II}-complexes

Treatment of Ni^{II}(OAc)₂·4H₂O and an equimolar amount of the ligands in methanol gave the corresponding Ni^{II}–acetate (OAc) complexes **1a–6a**. In the cases of **1a**,⁴² **2a**, **3a**, and **6a**, one of the two acetate ions, uncoordinated to nickel(II), was replaced by BPh₄⁻ by anion exchange reaction with NaBPh₄. The Ni^{II}–nitrate (NO₃) complexes **1b–4b** were also synthesized by the reaction of Ni^{II}(NO₃)₂·6H₂O and the ligands, and the uncoordinated NO₃⁻ was also replaced by BPh₄⁻ in a similar manner except in complex **3b**. All the complexes were paramagnetic (*S* = 1) as demonstrated by the ¹H NMR resonances spread over a chemical shift range of –20 to 70 ppm.^{42,51} Fig. 2 shows the ORTEP drawings of the

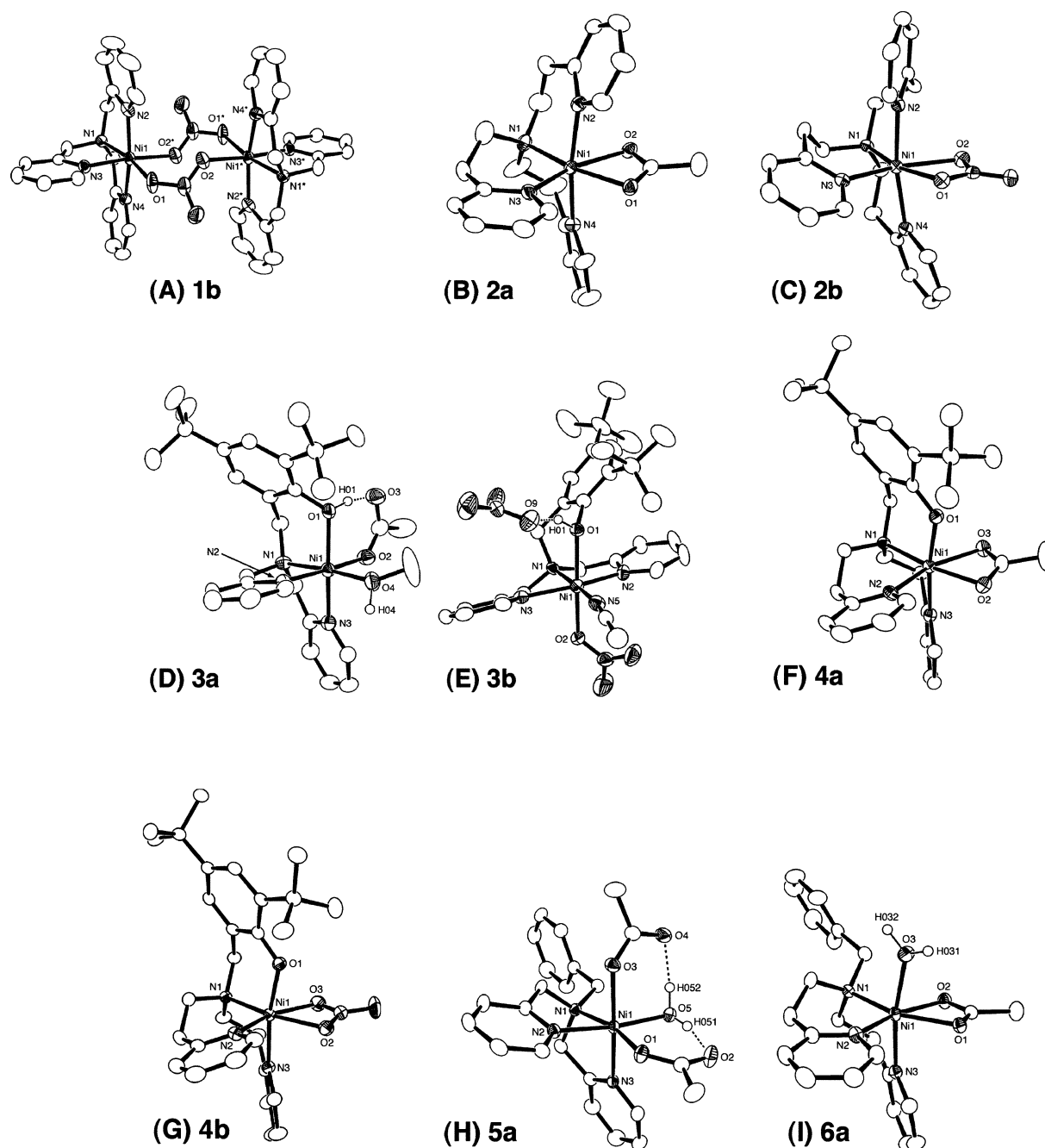


Fig. 2 ORTEP drawings of (A) $[\text{Ni}^{\text{II}}_2(\text{TPA})_2(\mu\text{-NO}_3)_2](\text{BPh}_4)_2$ (**1b**), (B) $[\text{Ni}^{\text{II}}(\text{TEPA})(\text{OAc})]\text{BPh}_4$ (**2a**), (C) $[\text{Ni}^{\text{II}}(\text{TEPA})(\text{NO}_3)]\text{BPh}_4$ (**2b**), (D) $[\text{Ni}^{\text{II}}(\text{D}^{\text{tbp}}\text{Pym}2\text{H})(\text{OAc})(\text{MeOH})]\text{BPh}_4$ (**3a**), (E) $[\text{Ni}^{\text{II}}(\text{D}^{\text{tbp}}\text{Pym}2\text{H})(\text{NO}_3)(\text{MeCN})]\text{NO}_3$ (**3b**), (F) $[\text{Ni}^{\text{II}}(\text{D}^{\text{tbp}}\text{Pye}2)(\text{OAc})]$ (**4a**), (G) $[\text{Ni}^{\text{II}}(\text{D}^{\text{tbp}}\text{Pye}2)(\text{NO}_3)]$ (**4b**), (H) $[\text{Ni}^{\text{II}}(\text{B}^2\text{Pym}2)(\text{OAc})_2(\text{H}_2\text{O})]$ (**5a**) and (I) $[\text{Ni}^{\text{II}}(\text{B}^2\text{Pye}2)(\text{OAc})(\text{H}_2\text{O})]\text{BPh}_4$ (**6a**) showing 50% probability thermal ellipsoids. The non-coordinating counter anion and the hydrogen atoms attached to the carbon atoms are omitted for clarity.

Ni^{II} -acetate complexes **2a–6a** and the Ni^{II} -nitrate complexes **1b–4b**, and the crystallographic data and the selected bond lengths and angles are presented in Tables S1 and S2,[†] respectively. The crystal structure of $[\text{Ni}^{\text{II}}(\text{TPA})(\text{OAc})(\text{H}_2\text{O})]\text{BPh}_4$ (**1a**) was reported in our previous communication.⁴²

Ni^{II} -TPA complex **1a** exhibits a mononuclear octahedral structure involving an acetate and a water molecule as the co-ligands.⁴² On the other hand, Ni^{II} -TPA complex **1b** prepared using $\text{Ni}^{\text{II}}(\text{NO}_3)_2 \cdot 6\text{H}_2\text{O}$ exhibits a dimeric structure consisting of a rare bis(μ -nitrate)dinickel(II) core, at the center of which there is an

inversion center of the complex [Fig. 2(A)]. The metal center shows a slightly distorted octahedral geometry with the N_4O_2 donor set, where the bond length of Ni–N(1) (alkylamine nitrogen, 2.0851 Å) is slightly longer than that of Ni–N_{py} [pyridine nitrogen N(2), N(3), and N(4), 2.0469, 2.0408, and 2.0547 Å, respectively], and the distance between Ni and O(2) (2.1233 Å) is somewhat longer than that of Ni–O(1) (2.0711 Å). The overall structure of **1b** is similar to that of $[\text{M}_2(\text{TPA})_2(\mu\text{-OAc})_2](\text{BPh}_4)_2$ (M = Fe^{II}, Mn^{II}).^{42,52}

Ni^{II} -TEPA complexes **2a** and **2b** exhibit a mononuclear structure involving a didentate acetate and nitrate co-ligand,

respectively, [Fig. 2(B) and 2(C)]. The complexes also have a distorted octahedral geometry with the N_3O_2 donor set, where the acetate ion in **2a** coordinates to Ni(II) unsymmetrically (Ni–O(1) = 2.0971 Å; Ni–O(2) = 2.1653 Å), whereas the nitrate ion in **2b** coordinates to the metal center fairly symmetrically (Ni–O(1) = 2.1576 Å; Ni–O(2) = 2.1676 Å). It should be noted that the average distance between the pyridine nitrogens and Ni(II) in **2a** (2.12 Å) is longer than that in **1a** (2.08 Å).⁴² Similarly, the average distances between the pyridine nitrogens and Ni(II) in **2b** (2.10 Å) is longer than that in **1b** (2.05 Å). These results unambiguously indicate that the coordinative interaction between the metal ion and the pyridine nitrogen in the TEPA-complexes is weaker than that in the TPA-complexes. This may cause an increasing Lewis acidity of Ni(II) in the TEPA-system as compared to that in the TPA-system, resulting in the different catalytic activity in the alkane hydroxylation reaction as reported in the following section.

The phenol ligand carrying the bis(2-pyridylmethyl)amine metal binding unit ^{Dtbp}Pym2H gave the corresponding mononuclear Ni(II)–phenol complexes **3a** and **3b**, in which the phenol moiety was not deprotonated (neutral phenol form is retained) [Fig. 2(D) and 2(E)].⁵³ Both complexes exhibit a similar octahedral geometry with the N_3O_3 donor set, in which two vacant sites are occupied by AcO^- and a methanol molecule in **3a** and by NO_3^- and an acetonitrile molecule in **3b**, although the relative positions of the two pyridine rings of the ligand is different. Namely, the pyridine donor groups occupy *cis* positions in **3a**, whereas *trans* positions in **3b** (**3a**: N(2)–Ni–N(3) = 96.35°; **3b**: N(2)–Ni–N(3) = 161.73°). The phenol proton in **3a** and **3b** forms hydrogen bonding interaction with the coordinating carboxylate oxygen (H(01)–O(3) 1.47 Å) and *non*-coordinating nitrate oxygen atoms (H(01)–O(9) 1.65 Å and H(05)–O(12) 1.87 Å), respectively. Formation of the *phenol* complexes clearly indicates the relatively low Lewis acidity of Ni(II) in the bis(2-pyridylmethyl)amine (Pym2) ligand system as mentioned above.

In contrast to the case of ^{Dtbp}Pym2H described above, another phenol ligand with the bis[2-(2-pyridyl)ethyl]amine (Pye2) metal binding moiety ^{Dtbp}Pye2H gave the corresponding *phenolate* complexes **4a** and **4b**, containing a didentate acetate and nitrate co-ligand, respectively [Fig. 2(F) and 2(G)]. In the case of complex **4a**, there were two structurally independent molecules (molecule 1 and molecule 2) in the crystal lattice, both of which showed a slightly distorted octahedral geometry. The Ni–O_{phenolate} bond is 1.987 Å in molecule 1 and 1.996 Å in molecule 2, which are shorter than the Ni–O_{phenol} bond (2.080 Å) of the phenol complex **3a**. Overall

structure of complex **4b** is similar to that of **4a**. Formation of the phenolate complexes **4a** and **4b** in the ^{Dtbp}Pye2H ligand system further demonstrates the higher Lewis acidity of Ni(II) in the bis[2-(2-pyridyl)ethyl]amine (Pye2) ligand system as compared with the bis(2-pyridylmethyl)amine (Pym2) ligand system just mentioned above.

Tridentate ligands ^{Bz}Pym2 and ^{Bz}Pye2 also afforded mononuclear Ni(II)–acetate complexes **5a** and **6a**, when they were treated with Ni^{II}(OAc)₂·4H₂O [Fig. 2(H) and 2(I)]. Both complexes exhibit octahedral geometry with N_3O_3 donor set. In the case of **5a**, the vacant sites are occupied by two monodentate acetate anions and one water molecule. The coordination of water molecule is stabilized by hydrogen bonding interactions between the hydrogen atoms of H₂O and carbonyl oxygen atoms of the acetate co-ligands (H(051)–O(2) 1.80 Å and H(052)–O(4) 1.73 Å). On the other hand, complex **6a** involves an acetate anion acting as a didentate co-ligand and the sixth coordination site is occupied by a water molecule. In this case, there is no intramolecular hydrogen bonding interaction stabilizing the coordination of H₂O.

The electronic absorption spectra of complexes **1a** and **6a** are shown in Fig. 3 as typical examples, and the spectral data (λ_{max} and ϵ) of all complexes are summarized in Table 1. Complex **1a** exhibits two broad absorption bands at 537 nm ($\epsilon = 19 M^{-1} cm^{-1}$) and 917 nm ($\epsilon = 22 M^{-1} cm^{-1}$) together with a very weak shoulder around 800 nm [Fig. 3(A)]. The spectrum is very close to that of

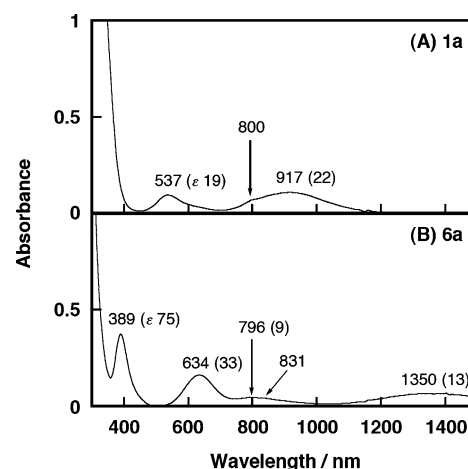


Fig. 3 UV-Vis spectra of (A) $[Ni^{II}(TPA)(OAc)(H_2O)]BPh_4$ (**1a**) and (B) $[Ni^{II}(\text{BzPye2})(OAc)(H_2O)]BPh_4$ (**6a**) in CH_2Cl_2 at 25 °C.

Table 1 UV-Vis data of the Ni^{II}-complexes in CH_2Cl_2 at 25 °C

Complex	Counter anion	λ_{max}/nm ($\epsilon/M^{-1} cm^{-1}$)
1a	OAc^-	537 (19), 800 (sh, 14), 917 (22)
1b^{a, b}	NO_3^-	540 (17), 783 (sh, 17), 868 (20)
2a	OAc^-	577 (18), 798 (sh, 2), 948 (7)
2b^a	NO_3^-	574 (32), 800 (sh, 4), 941 (9)
3a	OAc^-	410 (sh, 55), 591 (9), 780 (sh, 4), 962 (15)
3b	NO_3^-	400 (sh, 30), 579 (13), 782 (sh, 6), 964 (17)
4a	OAc^-	314 (6300), 595 (19), 794 (sh, 4), 977 (20)
4b	NO_3^-	311 (5700), 595 (25), 800 (sh, 7), 975 (23)
5a	OAc^-	606 (13), 770 (sh, 3), 1010 (13)
6a	OAc^-	389 (75), 634 (33), 796 (9), 831 (sh, 9), 1350 (13)

^a in CH_3CN . ^b the coefficients per one Ni²⁺ ion.

the octahedral nickel(II) complex of 2,6-bis[*bis*(2-pyridylmethyl)-amino]methyl-4-methylphenol (HBPMP) reported by Que, *et al.*⁵⁴ On the analogy of the reported data,⁵⁴ the lower energy band at 917 nm may be associated with the $^3A_{2g} \rightarrow ^3T_{2g}(F)$ transition, and the higher energy band at 537 nm can be assigned to the $^3A_{2g} \rightarrow ^3T_{1g}(F)$ transition. Then, the weak shoulder band around 800 nm can be ascribed to the spin-forbidden transition $^3A_{2g} \rightarrow ^1E_{1g}$. Thus, the spectral data suggest that complex **1a** retains the octahedral geometry in solution. All other complexes, except **6a**, exhibit similar electronic absorption spectra due to the d–d transitions (Table 1), indicating that those complexes also retain the octahedral geometry in solution. In addition to the d–d bands, complexes **3a** and **3b** show a weak band at ~ 400 nm ($\epsilon = 30\text{--}55$), which could be assigned to the phenol-to-Ni(II) charge transfer band, and phenolate complexes **4a** and **4b**, exhibit a phenolate-to-Ni(II) charge transfer band at ~ 310 nm ($\epsilon = \sim 6000$ M⁻¹ cm⁻¹).

Notably, the absorption spectrum of complex **6a** is different from those of the others. Namely, it shows five weak absorption bands at 389, 634, 796, 831 and 1350 nm [Fig. 3(B)], which are similar to the d–d bands of $^3B_1 \rightarrow ^3E$, $^3B_1 \rightarrow ^3E$, $^3B_1 \rightarrow ^3B_2$, $^3B_1 \rightarrow ^3A_2$ and $^3B_1 \rightarrow ^3E$, respectively, reported for the square pyramidal Ni(II) complexes.⁵⁵ Thus, the results indicate that complex **6a** exhibits a five-coordinated square pyramidal geometry in a non-coordinative solvent such as CH₂Cl₂. Thus, the weakly coordinated H₂O molecule in **6a** [see, Fig. 2(I)] may be dissociated in solution.

Catalytic activity in the alkane hydroxylation reaction with *m*-CPBA

In our previous communication,⁴² catalytic efficiency of a series of transition-metal (Ni^{II}, Co^{II}, Fe^{II} and Mn^{II}) complexes of TPA was examined in the hydroxylation reaction of cyclohexane with *m*-CPBA to demonstrate that the Ni^{II}(TPA) was the most preferable catalyst with respect to the total turnover number (TON) and the alcohol-product (A/K) selectivity. In this study, we have examined the effects of supporting ligands on the catalytic activity of nickel(II) complexes by changing (i) the alkyl linker chain length connecting the pyridine donor groups and the tertiary amine nitrogen [pyridylmethylamine (Pym) *vs.* pyridylethylamine (Pye)], (ii) the ligand donor atoms (pyridine nitrogen *vs.* phenol oxygen),

(iii) the denticity (tetradentate *vs.* tridentate) and (iv) the counter anion co-ligands (acetate *vs.* nitrate). In all the cases, the reaction proceeded catalytically to give cyclohexanol as the major product and cyclohexanone as the minor product as summarized in Table 2.

(i) **Effects of alkyl linker chain (Pym *vs.* Pye).** The time courses of TON (turnover number) of the catalysts **1a** and **2a** for the production of cyclohexanol and cyclohexanone are shown in Fig. 4 as a typical example. In the case of **1a** with the 2-pyridylmethylamine (Pym) tetradentate ligand (TPA), the catalytic reaction proceeded very effectively to reach the total TON of 656 (TON for cyclohexanol plus TON for cyclohexanone) after 60 min (entry 1).⁴² On the other hand, the reaction of **2a** with the 2-(2-pyridyl)ethylamine (Pye) tetradentate ligand was much slower (total TON = 265 after 60 min, entry 3), although the TON further increased at the prolonged reaction time (Fig. 4). Similarly, the catalytic efficiency of **3a** with phenol ligand ^{Dtbp}Pym2H containing the Pym metal-binding group (entry 5) is higher than that of **4a** with phenol ligand ^{Dtbp}Pye2H containing the Pye metal-binding moiety (entry 7) (also see Fig. S1†), and the catalytic efficiency of **5a** with tridentate ligand ^{Bz}Pym2 (entry 9) is higher than that

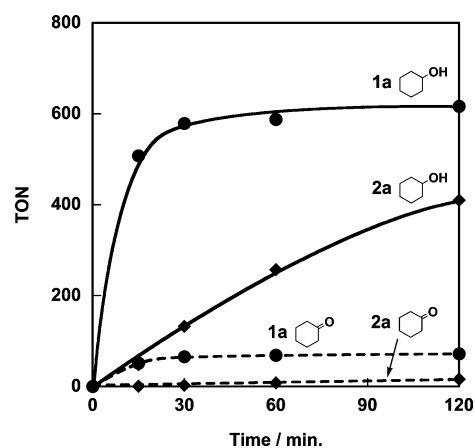


Fig. 4 Time courses for the oxidation of cyclohexane (2.5 M) catalyzed by (●) [Ni^{II}(TPA)(OAc)(H₂O)]BPh₄ (**1a**) (0.33 mM) and by (◆) [Ni^{II}(TEPA)(OAc)]BPh₄ (**2a**) (0.33 mM) in CH₂Cl₂–CH₃CN (v/v = 3 : 1, totally 6 ml) at room temperature.

Table 2 Oxygenation of cyclohexane with *m*-CPBA catalysed by the Ni^{II}-complexes^a

Entry	Complex	Counter anion	TON ^b		Total	A/K
			Cyclohexanol	Cyclohexanone ^c		
1	1a	OAc ⁻	587	69	656	8.5
2	1b	NO ₃ ⁻	544	68	612	8.0
3	2a	OAc ⁻	257	8	265	32.1
4	2b	NO ₃ ⁻	46	1	47	46.0
5	3a	OAc ⁻	657	88	745	7.5
6	3b	NO ₃ ⁻	567	61	628	9.3
7	4a	OAc ⁻	332	8	340	41.5
8	4b	NO ₃ ⁻	182	4	186	45.5
9	5a	OAc ⁻	455	69	524	6.6
10	6a	OAc ⁻	265	7	272	37.9

^a Reaction conditions; [Ni²⁺] = 0.33 mM, [*m*-CPBA] = 0.33 M, [cyclohexane] = 2.5 M in CH₂Cl₂–CH₃CN (3 : 1) at room temperature for 1 h under Ar.

^b Turnover number [(moles of product)/(moles of catalyst)] determined by GLC. ^c A small amount of ε-caprolactone was obtained as an over-oxidation product of cyclohexanone with *m*-CPBA.

of **6a** supported by tridentate ligand ^{Bz}Pye2 (entry 10) (also see Fig. S2†). From these results, it can be concluded that the catalytic efficiency (total TON) of the nickel(II) complexes involving the shorter methylene linker chain (Pym-system) is higher than that of the nickel(II) complexes with the longer ethylene linker chain (Pye-system).

With respect to the alcohol/ketone (A/K) selectivity, on the other hand, the Pye-ligand system (complexes **2a**, **2b**, **4a**, **4b**, and **6a**) gave much higher selectivity as compared to the Pym-ligand system (complexes **1a**, **1b**, **3a**, **3b**, and **5a**) (see Table 2). As seen in Fig. 4, the formations of cyclohexanol (A, solid line) and cyclohexanone (K, dashed line) are synchronized (there is no lag phase for the formation of K), demonstrating clearly that cyclohexanone (K) is NOT the over-oxidation product of cyclohexanol (A). In fact, the A/K value after 120 min (longer reaction time) is nearly the same as that after 60 min (shorter reaction time) in all the cases.

In our studies on the copper complexes of the same series of ligands, we have demonstrated that the electron-donating ability of pyridine donor group of the Pym-ligand system is higher than that of the Pye-ligand system.⁵⁶ The different electron-donor ability of the ligands may cause the difference in catalytic activity and A/K selectivity among the nickel(II) complexes as discussed below.

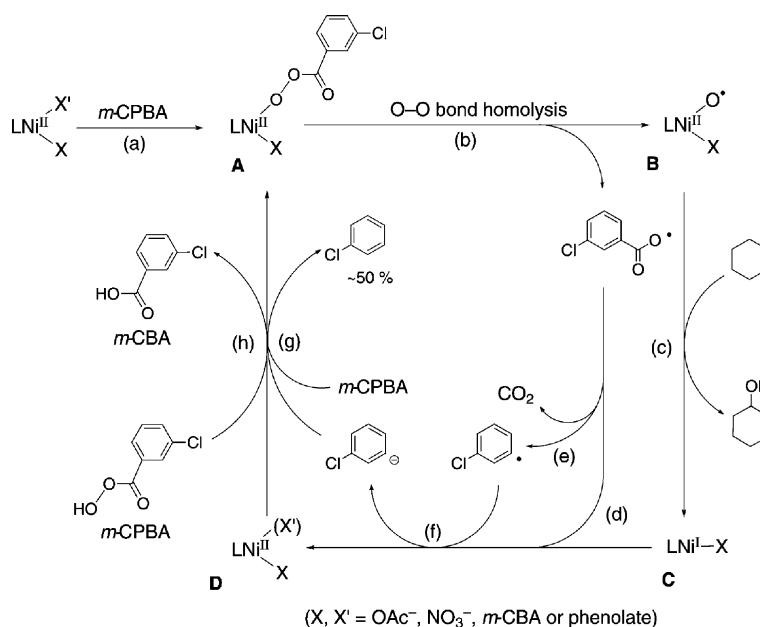
(ii) Effects of ligand donor atoms (pyridine nitrogen vs. phenol oxygen). The catalytic activity of the nickel(II) complexes with the phenol-containing ligands was higher than that of the corresponding tri-pyridine ligands [**3a** (745) vs. **1a** (656), **3b** (628) vs. **1b** (612), **4a** (340) vs. **2a** (265), **4b** (340) vs. **2b** (47)]. The higher electron-donor ability of the phenolate donor group as compared to the pyridine donor group may also cause the enhanced reactivity as mentioned above. In this respect, we assume that the phenol proton of complexes **3a** and **3b** is also dissociated during the catalytic cycle to give the corresponding phenolate complexes, although the phenol moiety of those complexes in the crystal is protonated (see Fig. 2(D) and 2(E)).

(iii) Effects of denticity (tetradentate vs. tridentate). The time courses of total TON for the reactions of **5a** and **6a**, which are supported by the tridentate ligand ^{Bz}Pym2 and ^{Bz}Pye2, respectively, are shown in Fig. S2.† The reaction profiles shown in Fig. S2† are similar to those of Fig. 4 for **1a** and **2a** with the tetradentate ligands TPA and TEPA, but the TONs of the tridentate ligand system are lower than those of the tetradentate ligand system. Thus, the reduction of the number of donor atoms from 4 to 3 resulted in the decrease of catalytic activity of the nickel(II) complexes.

(iv) Effects of counter anions. The counter anion effects on the reactions are shown in Fig. S3–S6.† A distinct lag phase was observed in the reactions catalyzed by the nitrate-complexes **1b**, **2b** and **3b**, whereas no such lag phase existed in the other cases. The counter anion co-ligands may contribute to the ligand exchange process with *m*-CPBA as discussed in the next section.

Mechanistic consideration

Although the mechanistic details of the catalytic reaction have yet to be clarified, a possible mechanism is shown in Scheme 1. First of all, *m*-CPBA reacts with the starting material $[(L)Ni^{II}(X)(X')]$ to give $[LNi^{II}(X)(OOC(O)Ar)]$ (**A**) [path (a)], where L is the supporting ligand, X and X' are the coordinated counter anion and/or the phenolate moiety involved in L and Ar is *m*-chlorophenyl group. Then, O–O bond homolysis may occur to give $[LNi^{II}(O\cdot)(X)]$ (**B**)⁵⁷ and $ArCO_2\cdot$ [path (b)], the former of which reacts with cyclohexane directly to give cyclohexanol product and $[LNi^I(X)]$ (**C**) [path (c)]. On the other hand, organic radical $ArCO_2\cdot$ readily reacts with $[LNi^I(X)]$ (**C**) to produce $[Ni^{II}(X)(OC(O)Ar)]$ (**D**) [path (d)] or releases CO_2 to give $Ar\cdot$ [path (e)] which may be reduced by $[LNi^I(X)]$ (**C**) [path (f)] and then protonated by another molecule of *m*-CPBA to produce *ArH* (chlorobenzene) and the *m*-CPBA adduct **A** [path (g)]. In fact, an appreciable amount of chlorobenzene (~50% based on the products) was obtained from



Scheme 1

the final reaction mixture. The ligand exchange reaction of *m*-CBA adduct **D** with another molecule of *m*-CPBA also regenerates the *m*-CPBA adduct **A** [path (h)], completing the catalytic cycle.

The higher electron-donor ability of pyridine in the Pym-ligand system as compared to the Pye-ligand system⁵⁶ may reduce Lewis acidity of the nickel(II) metal center, enhancing the ligand exchange processes [paths (a), (g) and (h)]. The phenolate ligand having higher electron-donor ability may have the same effect, further enhancing the ligand exchange processes. The higher electron-donating effect may also enhance the O–O bond cleavage of the *m*-CPBA adduct **A** to give reactive intermediate **B** [path (b)], also accelerating the catalytic reaction. These may be the reasons why the Pym-ligands and the phenolate ligands afforded higher catalytic activity (higher TON). The lower catalytic activity of the tridentate ligand system as compared to the tetradentate ligand system could be attributed to the less electron-donating ability of the tridentate ligands.

On the other hand, the Pye-ligands with lower electron-donor ability may enhance Lewis acidity of the nickel(II) metal center. This imparts the negative effect on the ligand exchange reactions as mentioned above. Nonetheless, the higher Lewis acidity of the metal center may enhance the inherent reactivity of nickel-oxo species **B** toward C–H bond activation of alkanes, thus resulting in the significantly high A/K selectivity in the Pye-ligand system. Que and his co-workers have suggested that the A/K selectivity increases as the reactivity of metal-oxo species becomes higher.⁵

The lag phase observed in the reactions with the nitrate-complexes **1b**, **2b** and **3b** might be due to the slow ligand exchange reaction between NO₃[−] and *m*-CPBA [path (a)]. In this process, the coordinated counter anion (AcO[−] and NO₃[−]) of the starting material may act as a proton acceptor from *m*-CPBA. Since the basicity of NO₃[−] is much lower than AcO[−], the ligand exchange process involving the deprotonation of *m*-CPBA may be slower with the nitrate-complexes as compared to the acetate-complexes. This may cause the lag phase in the early stage of the catalytic reaction with the nitrate-complexes. Once the complex goes into the catalytic cycle (after the lag phase), NO₃[−] is replaced by *m*-chlorobenzoic acid (*m*-CBA) in path (d), and thus, the catalytic reaction proceeded at nearly the same rate as the reaction of the acetate-complexes (Fig. S3–S6).†

In summary, we have examined the catalytic activity of the nickel(II) complexes of the series of pyridylalkylamine ligands in the hydroxylation reaction of cyclohexane with *m*-CPBA. It has been found that the catalytic activity (total TON) as well as the alcohol/ketone (A/K) selectivity of the nickel(II) complexes is significantly affected by the supporting ligands (Table 2). In general, complexes containing the pyridylmethylamine (Pym) metal-binding group (**1a**, **3a**, **5a**) showed higher turnover number (TON) than those containing the pyridylethylamine (Pye) metal-binding group (**2a**, **4a**, **6a**), whereas the alcohol/ketone (A/K) selectivity was much higher with the less reactive Pye-complexes. On the other hand, existence of NO₃[−] co-ligand caused a lag phase in the early stage of the catalytic reaction, which may be due to the slow ligand exchange reaction between NO₃[−] and *m*-CPBA in the initiation process of the catalytic cycle. Although direct evidence for the existence of nickel-oxo type reactive intermediate **B** (Scheme 1) has yet to be obtained, contribution of such a metal-based oxidant, rather than an auto-oxidation type free radical species, has been strongly suggested by the high A/K selectivity

and the high 3°/2° selectivity.^{5,42} We are now trying to detect the reactive intermediate using low temperature spectroscopic techniques.

Acknowledgements

This work was financially supported in part by Grants-in-Aid for Scientific Research (No. 17350086, 18037062, and 18033045) from the Ministry of Education, Culture, Sports, Science and Technology, Japan.

References

- 1 D. H. R. Barton and D. Doller, *Acc. Chem. Res.*, 1992, **25**, 504–512.
- 2 D. T. Sawyer, A. Sobkowiak and T. Matsushita, *Acc. Chem. Res.*, 1996, **29**, 409–416.
- 3 M. Fontecave, S. Ménage and C. Duboc-Toia, *Coord. Chem. Rev.*, 1998, **178–180**, 1555–1572.
- 4 A. E. Shilov and A. A. Shteinman, *Acc. Chem. Res.*, 1999, **32**, 763–771.
- 5 M. Costas, K. Chen and L. Que, Jr., *Coord. Chem. Rev.*, 2000, **200–202**, 517–544.
- 6 P. Stavropoulos, R. Çelenligil-Çetin and A. E. Tapper, *Acc. Chem. Res.*, 2001, **34**, 745–752.
- 7 K. Chen, M. Costas and L. Que, Jr., *J. Chem. Soc., Dalton Trans.*, 2002, 672–679.
- 8 T. Punniyamurthy, S. Velusamy and J. Iqbal, *Chem. Rev.*, 2005, **105**, 2329–2363.
- 9 *Metal-Oxo and Metal-Peroxo Species in Catalytic Oxidations*, ed. B. Meunier, Springer, Berlin, 2000.
- 10 A. Nanthakumar and H. M. Goff, *J. Am. Chem. Soc.*, 1990, **112**, 4047–4049.
- 11 H. Ohtake, T. Higuchi and M. Hirobe, *J. Am. Chem. Soc.*, 1992, **114**, 10660–10662.
- 12 T. Higuchi, K. Shimada, N. Maruyama and M. Hirobe, *J. Am. Chem. Soc.*, 1993, **115**, 7551–7552.
- 13 W. Nam, Y. M. Goh, Y. J. Lee, M. H. Lim and C. Kim, *Inorg. Chem.*, 1999, **38**, 3238–3240.
- 14 M. H. Lim, Y. J. Lee, Y. M. Goh, W. Nam and C. Kim, *Bull. Chem. Soc. Jpn.*, 1999, **72**, 707–713.
- 15 W. Nam, M. H. Lim, S.-Y. Oh, J. H. Lee, H. J. Lee, S. K. Woo, C. Kim and W. Shin, *Angew. Chem., Int. Ed.*, 2000, **39**, 3646–3649.
- 16 W. Nam, M. H. Lim, S. K. Moon and C. Kim, *J. Am. Chem. Soc.*, 2000, **122**, 10805–10809.
- 17 W. Nam, S.-E. Park, I. K. Lim, M. H. Lim, J. Hong and J. Kim, *J. Am. Chem. Soc.*, 2003, **125**, 14674–14675.
- 18 W. J. Song, Y. O. Ryu, R. Song and W. Nam, *J. Biol. Inorg. Chem.*, 2005, **10**, 294–304.
- 19 N. Kitajima, H. Fukui and Y. Moro-oka, *J. Chem. Soc., Chem. Commun.*, 1988, 485–486.
- 20 J. B. Vincent, J. C. Huffman, G. Christou, Q. Li, M. A. Nanny, D. N. Hendrickson, R. H. Fong and R. H. Fish, *J. Am. Chem. Soc.*, 1988, **110**, 6898–6900.
- 21 R. A. Leising, R. E. Norman and L. Que, Jr., *Inorg. Chem.*, 1990, **29**, 2553–2555.
- 22 N. Kitajima, M. Ito, H. Fukui and Y. Moro-oka, *J. Chem. Soc., Chem. Commun.*, 1991, 102–104.
- 23 R. H. Fish, M. S. Konings, K. J. Oberhausen, R. H. Fong, W. M. Yu, G. Christou, J. B. Vincent, D. K. Coggin and R. M. Buchanan, *Inorg. Chem.*, 1991, **30**, 3002–3006.
- 24 H.-C. Tung, C. Kang and D. T. Sawyer, *J. Am. Chem. Soc.*, 1992, **114**, 3445–3455.
- 25 R. A. Leising, J. Kim, M. A. Pérez and L. Que, Jr., *J. Am. Chem. Soc.*, 1993, **115**, 9524–9530.
- 26 S. Ménage, J. M. Vincent, C. Lambeaux, G. Chottard, A. Grand and M. Fontecave, *Inorg. Chem.*, 1993, **32**, 4766–4773.
- 27 S. Ménage, J. M. Vincent, C. Lambeaux and M. Fontecave, *J. Chem. Soc., Dalton Trans.*, 1994, 2081–2084.
- 28 M. Lubben, A. Meetsma, E. C. Wilkinson, B. Feringa and L. Que, Jr., *Angew. Chem., Int. Ed. Engl.*, 1995, **34**, 1512–1514.
- 29 J. Kim, R. G. Harrison, C. Kim and L. Que, Jr., *J. Am. Chem. Soc.*, 1996, **118**, 4373–4379.

- 30 M. Kodera, H. Shimakoshi and K. Kano, *Chem. Commun.*, 1996, 1737–1738.
- 31 C. Kim, K. Chen, J. Kim and L. Que, Jr., *J. Am. Chem. Soc.*, 1997, **119**, 5964–5965.
- 32 G. Roelfes, M. Lubben, R. Hage, L. Que, Jr. and B. L. Feringa, *Chem.–Eur. J.*, 2000, **6**, 2152–2159.
- 33 K. Chen and L. Que, Jr., *J. Am. Chem. Soc.*, 2001, **123**, 6327–6337.
- 34 J. Kaizer, E. J. Klinker, N. Y. Oh, J.-U. Rohde, W. J. Song, A. Stubna, J. Kim, E. Münck, W. Nam and L. Que, Jr., *J. Am. Chem. Soc.*, 2004, **126**, 472–473.
- 35 G. B. Shul'pin, C. C. Golfeto, G. Süß-Fink, L. S. Shul'pina and D. Mandelli, *Tetrahedron Lett.*, 2005, **46**, 4563–4567.
- 36 B. R. Cook, T. J. Reinert and K. S. Suslick, *J. Am. Chem. Soc.*, 1986, **108**, 7281–7286.
- 37 K. Jitsukawa, Y. Oka, S. Yamaguchi and H. Masuda, *Inorg. Chem.*, 2004, **43**, 8119–8129.
- 38 W. Nam, I. Kim, Y. Kim and C. Kim, *Chem. Commun.*, 2001, 1262–1263.
- 39 W. Nam, J. Y. Ryu, I. Kim and C. Kim, *Tetrahedron Lett.*, 2002, **43**, 5487–5490.
- 40 M. Yamaguchi, H. Kousaka, S. Izawa, Y. Ichii, T. Kumano, D. Masui and T. Yamagishi, *Inorg. Chem.*, 2006, **45**, 8342–8354.
- 41 C. Shimokawa, J. Teraoka, Y. Tachi and S. Itoh, *J. Inorg. Biochem.*, 2006, **100**, 1118–1127.
- 42 T. Nagataki, Y. Tachi and S. Itoh, *Chem. Commun.*, 2006, 4016–4018.
- 43 D. Schröder and H. Schwarz, *Angew. Chem., Int. Ed. Engl.*, 1995, **34**, 1973–1995.
- 44 W. L. F. Armarego and D. D. Perrin, *Purification of Laboratory Chemicals 4th edn*, Butterworth-Heinemann, Oxford, 1996.
- 45 Z. Tyeklár, R. R. Jacobson, N. Wei, N. N. Murthy, J. Zubieta and K. D. Karlin, *J. Am. Chem. Soc.*, 1993, **115**, 2677–2689.
- 46 M. Schatz, M. Becker, F. Thaler, F. Hampel, S. Schindler, R. R. Jacobson, Z. Tyeklár, N. N. Murthy, P. Ghosh, Q. Chen, J. Zubieta and K. D. Karlin, *Inorg. Chem.*, 2001, **40**, 2312–2322.
- 47 B. de Bruin, J. A. Brands, J. J. M. Donners, M. P. J. Donners, R. de Gelder, J. M. M. Smits, A. W. Gal and A. L. Spek, *Chem.–Eur. J.*, 1999, **5**, 2921–2936.
- 48 I. Sanyal, M. Mahroof-Tahir, M. S. Nasir, P. Ghosh, B. I. Cohen, Y. Gultneh, R. W. Cruse, A. Farooq, K. D. Karlin, S. Liu and J. Zubieta, *Inorg. Chem.*, 1992, **31**, 4322–4332.
- 49 Y. Shimazaki, S. Huth, S. Hirota and O. Yamauchi, *Bull. Chem. Soc. Jpn.*, 2000, **73**, 1187–1195.
- 50 S. Itoh, M. Taki, H. Kumei, S. Takayama, S. Nagatomo, T. Kitagawa, N. Sakurada, R. Arakawa and S. Fukuzumi, *Inorg. Chem.*, 2000, **39**, 3708–3711.
- 51 E. Szajna, P. Dobrowolski, A. L. Fuller, A. M. Arif and L. M. Berreau, *Inorg. Chem.*, 2004, **43**, 3988–3997.
- 52 S. Ménage, Y. Zang, M. P. Hendrich and L. Que, Jr., *J. Am. Chem. Soc.*, 1992, **114**, 7786–7792.
- 53 Shimazaki and co-workers reported the Ni(II)-chloride complex of ^{Dtbp}Pym2H, where the phenol moiety of the ligand was deprotonated, providing a phenolate complex; Y. Shimazaki, S. Huth, S. Karasawa, S. Hirota, Y. Naruta and O. Yamauchi, *Inorg. Chem.*, 2004, **43**, 7816–7822.
- 54 T. R. Holman, M. P. Hendrich and L. Que, Jr., *Inorg. Chem.*, 1992, **31**, 937–939.
- 55 (a) M. Ciampolini, *Inorg. Chem.*, 1966, **5**, 35–40; (b) A. T. Phillip, W. Mazurek and A. T. Casey, *Aust. J. Chem.*, 1971, **24**, 501–511; (c) S. V. Kryatov, B. S. Mohanraj, V. V. Tarasov, O. P. Kryatova, E. V. Rybak-Akimova, B. Nuthakki, J. F. Rusling, R. J. Staples and A. Y. Nazarenko, *Inorg. Chem.*, 2002, **41**, 923–930.
- 56 S. Itoh and Y. Tachi, *Dalton Trans.*, 2006, 4531–4538.
- 57 Intermediate **B** could also be drawn as [LNi^{III}=O(X)]. Mechanistic details including the structure of **B** are now under investigation.